DMD Fast Forward. Published on May 31, 2007 as doi:10.1124/dmd.107.014746

DMD#14746

IN VITRO METABOLIC STUDY OF TEMSIROLIMUS: PREPARATION, ISOLATION, AND IDENTIFICATION OF THE METABOLITES

Ping Cai, Rushung Tsao, and Mark E. Ruppen

Chemical and Pharmaceutical Development,
Wyeth Research, 401 N. Middletown Road, Pearl River, NY 10965

DMD Fast Forward. Published on May 31, 2007 as DOI: 10.1124/dmd.107.014746
This article has not been copyedited and formatted. The final version may differ from this version.

Running Title:

IN VITRO METABOLIC STUDY OF TEMSIROLIMUS

Corresponding Author:
Name: Ping Cai,
Address: Wyeth Research, Building 250/229,
401 N. Middletown Road, Pearl River, NY 10965
Telephone: 845-602-5261
Fax: 845-602-5592
E-mail: caip@wyeth.com.

Number of Text Pages: 20

Number of Tables: 5

Number of Figures: 12

Number of References: 14

Number of Words for Abstract: 195

Number of Words for Introduction: 188

Number of Words for Discussion: 703

Abbreviations: Temsirolimus, rapamycin-42-[2,2-bis-(hydroxymethyl)]-propionate; HLM, human liver microsomes; LC-MS, liquid chromatography-mass spectrometry; MS/MS, tandem mass spectrometry; CID, collision induced dissociation.

DMD Fast Forward. Published on May 31, 2007 as DOI: 10.1124/dmd.107.014746
This article has not been copyedited and formatted. The final version may differ from this version.

ABSTRACT:

The *in vitro* metabolism of temsirolimus, {rapamycin-42-[2,2-bis-(hydroxymethyl)]-propionate}, an antineoplastic agent, was studied using human liver microsomes as well as recombinant human P450s, namely CYP-3A4, 1A2, 2A6, 2C8, 2C9, 2C19, and 2E1. Fifteen metabolites were detected by liquid chromatography-tandem mass spectrometry. CYP3A4 was identified as the main enzyme responsible for the metabolism of the compound. Incubation of temsirolimus with recombinant CYP3A4 produced most of the metabolites detected from incubation with human liver microsomes, which was used for large-scale preparation of the metabolites. By silica gel chromatography followed by semi-preparative reverse-phase HPLC, individual metabolites were separated and purified for structural elucidation and bioactivity studies. The minor metabolites (peak 1-7) were identified as hydroxylated or demethylated macrolide ring-opened temsirolimus derivatives by both positive and negative MS and MS/MS spectroscopic methods. Since these compounds were unstable and only present in trace amounts, no further investigations were conducted. Six major metabolites were identified as 36-hydroxyl temsirolimus (M8), 35-hydroxyl temsirolimus (M9), 11-hydroxyl temsirolimus with an opened hemi-ketal ring (M10 and M11), N-oxide temsirolimus (M12), and 32-O-desmethyl temsirolimus (M13) using combined LC-MS, MS/MS, MS/MS/MS and NMR techniques. Compared to the parent compound, these metabolites showed dramatically decreased activity against LNCaP cellular proliferation.

Introduction

Temsirolimus {sirolimus-42-[2,2-bis-(hydroxymethyl)]-propionate}is an ester analog of rapamycin (Figure 1), a natural macrolide antibiotic with antifungal, antitumor, and immunosuppressive activities (Sehgal et al., 1994). Temsirolimus has demonstrated significant inhibition of tumor growth both *in vitro* and *in vivo*. It binds to the cytoplasmic protein FKBP forming a complex that antagonizes the mTOR (mammalian target of rapamycin) signaling pathway (Peralba et al., 2003). This consequently inhibits many of the downstream processes affected by mTOR kinase activity, including transcriptional and translational control of important cell-cycle regulators, resulting in cell cycle arrest (Sehgal 1995). Temsirolimus is currently in phase III clinical development for the treatment of the patients with renal cancer.

Although CYP3A4 had been identified as the major enzyme involved in the formation of the main metabolite of rapamycin, 41-O-desmethyl rapamycin, (Sattler et al., 1992; Christiants et al., 1992, Wang et al. 1994), little additional information about rapamycin metabolism has been reported due to the complexity of the metabolic profile and the instability of the metabolites.

The objective of this study was to identify the human P450 enzymes involved in temsirolimus metabolism, isolate and characterize the major metabolites, and evaluate their antitumor activities.

Materials and Methods

Chemicals and Reagents. Temsirolimus and recombinant P450s (3A4, 1A2, 2A6, 2C8, 2C9, and 2E1) were obtained from the Bioprocess Department of Wyeth Research (Pearl River, NY). Human liver microsomes were purchased from BD Biosciences (6

Henshaw St. Worburn, MA). Reagents for the NADPH generation system (disodium salt of NADP, D-glucose-6-phosphate, and glucose-6-phospate dehydrogenase) were purchased from Sigma Chemical Co. (St. Louis, MI). Other reagent-grade chemicals and HPLC-grade solvents were purchased from EM Science (Gibbstown, NJ) or J. T. Baker (Phillisburg, NJ).

Incubation of Temsirolimus with Human Liver Microsomes. Temsirolimus (50 μM) was incubated with 1 mg/ml of human liver microsomal proteins in 0.1 M phosphate buffer solution (pH 7.4) containing 1 mM EDTA and 4 mM of $MgCl_2$. Reactions were initiated by addition of the NADPH-regenerating system, resulting in a final concentration of 4 mM glucose-6-phosphate, 2 mM NADP, and 1 unit/ml of glucose-6-phosphate dehydrogenase. The incubations were carried out at 37^{o}C in a shaking water bath. Control incubations without the NADPH-regenerating system were performed under the same conditions. The reactions were terminated by the addition of cold acetonitrile. Precipitated materials were removed by centrifugation at 5000 rpm for 10 min at 4^{o}C, and the supernatants were collected and dried under vacuum. The dried extracts containing the metabolites were reconstituted in acetonitrile/water (7:3) for HPLC and LC-MS analysis.

Incubation of Temsirolimus with Recombinant Human P450s. Selected recombinant P450s (3A4, 1A2, 2A6, 2C8, 2C9, and 2E1, 0.3 *n*mol each) were individually incubated with temsirolimus (50 μM). The other components of the reaction mixtures were the same as above for the incubation of human liver microsomes. After incubation for 40 min at 37^{o}C, the reactions were quenched with cold acetonitrile. Subsequent sample treatment was the same as for the human liver microsomes samples.

Chemical Inhibition of P450 3A4 Activities. Ketoconazole in ethanol (10 μl) was added to each tube containing the human liver microsomes (1 mg/ml), EDTA (1 mM), $MgCl_2$ (4 mM), temsirolimus (50 μM) and 0.1 M potassium phosphate buffer (pH 7.4), giving a total reaction volume of 900 μl. The final concentration of ketoconazole in the assays ranged from 1 to 100 μM. Duplicate samples were prepared at each concentration. The samples were pre-incubated for 2 min at 37^{o}C, then 100 μl of an NADPH-regenerating system (same as described above) was added to initiate the reactions. The reactions were incubated at 37^{o}C for 15 min, and then quenched with cold acetonitrile. Subsequent sample processing was the same as described above.

Large-scale Preparation of Temsirolimus Metabolites. The large-scale incubation was conducted in a 5 liter reactor containing temsirolimus (400 mg in 10 ml ethanol), recombinant CYP3A4 (1200 nmol), $MgCl_2$ (400 mM x 40 ml), and NADPH regenerating system (final concentration: 4 mM of glucose-6-phosphate, 1.6 mM NADP, and 0.6 unit/ml of glucose-6-phosphate dehydrogenase) in 0.1 M potassium phosphate buffer for a total volume of 4 liter. The incubation was conducted under oxygen (bubbled O_2 at 0.30 L/min) with agitation at 125 rpm. After incubation for 60 min at 37°C, the mixtures were cooled to 25°C, and then extracted twice with equivalent volumes of ethyl acetate. The ethyl acetate extracts were combined after solvent was evaporated under vacuum to yield about 1 gram of crude extract.

Isolation of the Metabolites from Large-scale Preparation. The crude extract was dissolved in 4 ml acetone and loaded onto a silica gel flash column. The column was sequentially eluted with hexane/acetone and acetone/methanol gradients. A total of 20 fractions were collected (350 ml/fraction) and analyzed by LC-MS. Fractions 1 to 9

consisted mainly of lipids from the CYP3A4 membranes (176 mg); fractions 9 to12 contained unmodified temsirolimus (290 mg); fractions 13 to 17 contained the temsirolimus metabolites (96 mg); and fractions 18-20 contained the polar pigments from the membranes (145 mg). Fractions 13 to17 were combined for further separation by semi-preparative HPLC on a Supelcosil LC-18 column (10 x 250 mm, 5 μm). A stepwise gradient consisting of methanol:water with 5 mM ammonium acetate was used at a flow rate of 2.0 ml/min (methanol from 60% to 70% in 30 min and from 70% to 82% in 60 min). Separation was monitored by UV detector at both 220 nm and 280 nm. Each metabolite was collected in a separate container on ice as it eluted from the HPLC column. After the organic solvents were removed by vacuum evaporation, the aqueous residues were lyophilized to provide the purified individual metabolites.

HPLC, LC-MS, MS/MS and NMR Methods. Analytical HPLC was conducted using a Waters Alliance model 2690 HPLC with a Supelcosil LC-C18 analytical column (4.6 x 250 mm, 5 μm). A gradient of methanol:water with 5 mM ammonium acetate was used as the mobile phase at a flow rate of 0.6 ml/min (methanol from 65% to 85% in 70 min). Semi-preparative HPLC was performed on a Supelcosil LC-C18 semi-preparative column (10 x 250 mm, 5 μm). A step gradient of water containing 5 mM ammonium acetate:methanol was used as the mobile phase. The gradient was started from 60% methanol and increased linearly to 70% methanol in 30 min, followed by increasing methanol to 82 % in 60 min and holding for 5 min. The flow rate of the mobile phase was set at 2 ml/min.

LC-MS analysis was performed on an Agilent 1100 HPLC connected via 0.005" ID peek tubing to a MSD1100 mass spectrometer. The above-mentioned analytical HPLC

conditions were also applied to LC-MS analysis and half of the solvent was channeled into the mass spectrometer. Full scan atmospheric pressure chemical ionization (APCI) and electro-spray ionization (ESI) mass spectra were acquired at unit resolution from m/z 200 to 1200 at a step of 0.2. The negative ion mode was recorded.

The MS/MS/CID spectra of the purified metabolites were obtained on an Applied Biosystems-PE Sciex QSTAR PULSAR quadrupole time-of flight tandem mass spectrometer coupled with a Shimadzu-10Advp HPLC system. Electro-spray ionization was conducted in both negative and positive modes. MS/MS/CID experiments were carried out using the collision energies from –45 to –50V in the negative mode. For the positive mode, the collision energies were used in a range of 30 to 50 V, depending on the molecular structures. For temsirolimus and analogues, the collision energy was 50 V, but the macrolide ring-opened molecules (seco-temsirolimus type derivatives), the collision energy was 30V or lower (the molecular ion was not detectable if the CID energy > 30 V). Temsirolimus was used as the internal reference to measure the exact mass of the metabolite' molecular ion for elemental composition calculation. MS/MS fragment ions and their corresponding elemental compositions were calculated using the measured molecular ion as well as a common known fragment ion as references.

The LC-NMR data of M8 were acquired on a 600 MHz Bruker DRX spectrometer equipped with a single flow-cell LC-NMR probe. The LC-separation was performed on an XTerra column (4.6 x 250 mm, 5 μm) with a mobile phase of D_2O and acetonitrile-d_3 (acetonitrile-d_3 from 50% to 90% in 20 min at a flow rate of 0.6 ml/min). Proton spectra were collected with double-solvent suppression. For the other metabolites, the ^{1}H-NMR data were acquired on a 500 MHz Bruker DRX 500 spectrometer in acetonitrile-d_3.

Results

Temsirolimus Metabolism with Human Liver Microsomes and Recombinant CYP3A4. Incubation of temsirolimus with human liver microsomes in the presence of the NADPH regenerating system indicated that the total metabolite concentration reached a maximum after 40 minutes. At that time, the concentration of temsirolimus was reduced by 22±3%, which included its conversion to the macrolide ring opened product, seco-temsirolimus (12±3%, Fig. 1). A representative HPLC chromatogram of the metabolites generated by human liver microsomes is shown in Figure 1b. The major peak at 25.6 min, which is also observed in the control samples, is seco-temsirolimus identified by direct LC-MS comparison with the authentic standard. Since it was also present in the control samples, this compound was considered to be a no-specific degradation product resulted from a hydrolysis of the macrocyclic lactone ring followed by dehydration of C_{25}/C_{26}. The same ring-opening product, seco-rapamycin, had also been detected from the incubation of rapamycin with human liver microsomes and the pooled bile of intravenously dosed rats (Wang et al., 1997). Same as seco-rapamycin, seco-temsirolimus did not show any antitumor and FKBP binding activities due to the macrolide ring opening. Compared to the control incubation (Fig. 1a), fifteen new peaks appeared in the human liver microsomes reaction. Peaks 1 to 7, peak 11′, and peak 14 were the minor products, observed at trace levels (each peak area was < 0.3% of the total HPLC area of the analyzed sample). Peaks 8 (2.6%), 9 (0.43%), 10 (0.68%), 11 (0.82%), 12 (0.40%), and 13 (0.88%) were the major metabolites designated as M8 through M13 for convenience. The formation of these new peaks was inhibited by bubbling CO through the reaction solution during incubation (data not shown). This observation suggested that

biotransformation of temsirolimus required the presence of microsomal CYP450 monooxygenases.

To identify the enzymes involved in biotransformation, temsirolimus was individually incubated with each of six recombinant human P450 enzymes: 1A2, 2A6, 3A4, 2C8, 2C9, and 2E1. Experimental results indicated that recombinant CYP3A4 generated almost all of the metabolites detected in the human liver microsome studies, with the exception of peak 11′, which is shown in Fig. 1c. No significant metabolism was noted in any of the other recombinant CYP450 reactions.

Further comparison of the metabolic products produced by human liver microsomes and by recombinant CYP3A4 was also carried out by LC-MS. After the metabolites were separated and collected from semi-preparative HPLC, each individual metabolite peak was analyzed by LC-MS. The semi-preparative HPLC chromatograms of the metabolic products from human liver microsomes and from incubation with recombinant CYP3A4 are shown in Fig. 2 and the LC-MS results were summarized in Table 1. The major metabolites (M8 to M13) produced in human liver microsomes and in recombinant CYP3A4 incubations displayed close similar retention times and the same molecular ions.

Inhibition of Temsirolimus Metabolism. Ketoconazole, an antifungal drug, is a potent inhibitor of CYP3A4 (Maurice et al., 1992). The addition of ketoconazole to the reaction inhibited the biotransformation of temsirolimus by human liver microsomes. The effect of ketoconazole on the formation of the major metabolites is shown in Fig. 3. Ketoconazole inhibited the formation of metabolites M8 through M13 with an IC_{50} < 2μM. The addition of 5 μM ketoconazole decreased metabolite formation to 10-20% of

DMD Fast Forward. Published on May 31, 2007 as DOI: 10.1124/dmd.107.014746
This article has not been copyedited and formatted. The final version may differ from this version.

control levels. This result confirmed that CYP3A4 was the main enzyme responsible for the biotransformation of temsirolimus.

Isolation and Structure Elucidation of Temsirolimus Metabolites. In order to obtain enough material for structural elucidation and antitumor activity studies, a 4-liter reaction was performed by incubating 400 mg of temsirolimus with 1200 nmol CYP 3A4 and the NADPH regenerating system. After solvent extraction, the crude extract was subjected to silica gel fractionation to eliminate the un-reacted starting compound and the impurities from CYP3A4 membranes. The crude metabolite mixture was then separated by semi-preparative HPLC to yield purified individual metabolites for structure elucidation.

The minor components appearing before seco-temsirolimus in the preparative HPLC chromatogram (peaks 1-6, Fig. 2) were either hydroxylated or demethylated temsirolimus derivatives, as suggested by their molecular ions listed in Table 1. For example, the peak with $[M-H]^-$ at *m/z* 1060 was a dihydroxylated temsirolimus derivative, the peak with $[M-H]^-$ at *m/z* 1044 was a monohydroxylated temsirolimus derivative, and the peak with $[M-H]^-$ at *m/z* 1046, was either a desmethyl-dihydroxyl temsirolimus or a temsirolimus ester bond hydrolysis product. Like seco-temsirolimus, these components easily fragmented in the positive MS/MS/CID mode (i.e. fragmentation at lower collision energy, ≤ 30 V), suggesting that they were macrolide ring-opened derivatives (open at the O_{24}/C_{25} bond). Peak 7 from both human liver microsomes incubation and recombinant CYP3A4 incubation exhibited an $[M-H]^-$ at *m/z* 1030 and was identified as a C_{27} ketone reduced seco-temsirolimus (C=O converted to CH-OH) by its MS/MS and MS/MS/MS spectra. Considering that these compounds were unstable, their abundances were very low, and no

biological activity due to the ring-opening, further structural study was not performed on them. Structure elucidation by MS/MS, MS/MS/MS, and NMR focused on the major metabolites: M8, M9, M10, M11, M12 and M13.

MS/MS Fragmentation of Temsirolimus. Temsirolimus exhibited a molecular ion at *m/z* 1028 in the negative ESI-MS spectrum, which gave two fragment ions at *m/z* 590 and *m/z* 437 in the MS/MS/CID experiment. These two ions resulted from cleavage of the C_{31}/C_{32} bond and the O_{24}/C_{25} ester bond, representing the 'southern' portion and the 'northern' portion of the molecule, respectively (Fig. 4). These characteristic cleavages were also observed in rapamycin and its analogues. Via loss of neutral species, such as H_2O, MeOH, and /or CO_2, the 'northern' portion generated the fragment ions of *m/z* 407, *m/z* 389, and *m/z* 371, and the 'southern' portion produced the fragment ions of *m/z* 546, *m/z* 528, *m/z* 514, and *m/z* 496, which are designated as "group-1" ions in Table 2. Further cleavage of the 'southern' part at C_8/C_9 and C_{35}/C_{36} (allylic cleavage) followed by loss of methanol gave rise to the fragment ions at *m/z* 261, *m/z* 229, and *m/z* 147. β-cleavage of C_{33} ketone in the 'southern' part produced the fragment ion of *m/z* 101. All these fragment ions from the right region of the 'southern' part are classified as "group-2" ions in Table 2. The ion at *m/z* 252 was formed by C_8/C_9 cleavage followed by CO_2 loss (cleavage at C_{22}/C_{23}) in the left region of the 'southern' portion. The ion at *m/z* 234 resulted from a further loss of H_2O. The additional fragment ions at *m/z* 168 and *m/z* 128 arised from cleavages occurring at C_{13}/C_{15} and C_{23}/O_{24}, and cleavage of the amide bond (C_{16}/N_{17}) in the 'southern' part, respectively (Fig. 4). These ions (*m/z* 252, *m/z* 234, *m/z* 168, and *m/z* 128) from the left region of the 'southern' part are assigned as "group-3" in Table 2. All the fragmentation assignments described are shown in Fig. 4, which were

achieved by accurate mass measurements, MS/MS/MS analysis of the fragment ions at *m/z* 590 and *m/z* 261, and comparison with the MS/MS data of rapamycin. These fragment ions were used as the diagnostic criteria for structural elucidation of the metabolites by the mass shift technique. For example, the presence of the *m/z* 437 fragment ion in a metabolite indicated that the 'northern' portion of the molecule was intact. The disappearance of the group-2 fragment ions at *m/z* 261, *m/z* 229 and *m/z* 147 indicated that biotransformation had occurred in the C_1-C_8 region and /or the C_{36} position of the 'southern' portion. Using this technique, the locations of biotransformation were determined. Table 2 listed the fragment ions observed in the MS/MS/CID spectra of temsirolimus and its metabolites.

Identification of M8. M8 showed a deprotonated molecular ion at *m/z* 1044 in the ESI-MS spectrum, 16 Daltons higher than that of temsirolimus, indicating a mono-hydroxylation (or oxidation) product of temsirolimus. The hydroxylation occurred at the 'southern' part of the molecule as suggested by the intact 'northern' fragment ions at *m/z* 437 and the modified 'southern' fragment ion at *m/z* 606 in MS/MS spectrum (Table 2). Compared with the parent compound, which showed the group-2 ions at *m/z* 261, *m/z* 229, *m/z* 147 and *m/z* 101, M8 gave the fragment ions at *m/z* 277, *m/z* 245, *m/z* 163, and *m/z* 101 (Table 2), suggesting that hydroxylation had occurred on the right side of the 'southern' part, of either C_{36} or the C_1-C_8 moiety (Fig. 5a). Since M8 displayed the same UV absorption as temsirolimus, the triene group (C_1-C_6) should be unchanged, thus limiting the possible biotransformation positions to C_7, C_8, C_{36}, and two methyl groups. M8 was finally identified as 36-hydroxyl temsirolimus by LC-NMR. In the ^{1}H-NMR spectrum of M8 (Fig. 5b), the disappearance of H_{36} resonance and the significant

DMD Fast Forward. Published on May 31, 2007 as DOI: 10.1124/dmd.107.014746
This article has not been copyedited and formatted. The final version may differ from this version.

downfield shifts of H_1 (δ 5.66 ppm) as compared with temsirolimus (δ 5.46 ppm) suggested a 36-hydroxylation structure for M8. Since hydroxylation would eliminate H_{36}, the C_{36}-methyl proton of M8 would present as the observed singlet at δ1.22 ppm instead of a doublet at δ 0.89 ppm in ^{1}H-NMR of temsirolimus, corroborating the proposed structure of M8.

Identification of M9. M9 also showed a deprotonated $[M-H]^-$ at *m/z* 1044 and the fragment ions at *m/z* 437 and *m/z* 606 in the negative ESI mass spectrum, suggesting a 'southern' hydroxylation derivative of temsirolimus. In MS/MS/CID experiment, M9 displayed the same group-3 fragment ions (*m/z* 252, *m/z* 234, *m/z* 168, and *m/z* 128, Table 2) as the parent compound, indicating that the 'southern' left portion (C_9-C_{23}) had been left intact. The appearance of the group-2 ions at *m/z* 277, *m/z* 245, *m/z* 227, and *m/z* 147 (Table 2) suggested that biotransformation had occurred in the C_{32}-C_{35} region (Fig. 6). Like temsirolimus and M8, M9 also showed a fragment ion at m/z 101 due to the cleavage of C_{34}/C_{35} in the 'southern' part, suggesting that the C_{32}-C_{34} region was intact and hydroxylation had occurred at C_{35}. The observation of unique ions at *m/z* 504, *m/z* 472, and *m/z* 175 supported this suggestion (Table 2). On the basis of the accurate mass measurement and elemental composition analysis (Table 3), these ions were assigned and shown in Fig. 6. The *m/z* 504 ion resulted from the loss of the C_{32}-C_{34} moiety of the 'southern' part. Further elimination of MeOH or subsequent cleavage at C_8/C_9 followed by MeOH loss resulted in the fragment ions at *m/z* 472 and *m/z* 175 (Fig. 6), respectively.

Identification of M10 and M11. M10 was also a 'southern' oxygenated derivative of temsirolimus, as suggested by the appearance of the same 'northern' ions as for temsirolimus, but different 'southern' ions in the MS/MS spectrum (Table 2). The same

group-2 fragment ions (*m/z* 261, *m/z* 229, and *m/z* 147) seen for temsirolimus were also found in the M10 spectrum, which excluded the possibility of biotransformation at the 'southern' right region from C_1 to C_8 and C_{36} to C_{32} (Fig. 7). The observation of the group-3 ions at *m/z* 168 (due to the cleavage of C_{13}/C_{15} and C_{23}/O_{24}), and *m/z* 128 (due to the cleavage of the amide bond in the 'southern' part) indicated that the upper left region from C_{15} to O_{24} of the 'southern' part was also intact. The appearance of unique ions at *m/z* 196, *m/z* 240, *m/z* 289, and *m/z* 321 (Table 2) indicated that the hemiketal ring opened and the most likely hydroxylation position was C_{11}. The hydroxylation of C_{11} led to C_{11}/C_{12} cleavage in the 'southern' portion to form the highest intensity fragment ion at *m/z* 240 (Fig. 7). Further loss of CO_2 gave rise to the fragment at *m/z* 196. C_{11}-hydroxylation also facilitated the cleavage of the C_9/C_{10} bond, giving the fragment ion at *m/z* 321, which went on to lose MeOH for a strong peak at *m/z* 289 (Fig. 7). The same fragmentation pattern had also been observed in the MS/MS/CID spectrum of 11-hydroxyl rapamycin from a previous study we had conducted. For M10, the hemiketal ring opening increased the flexibility of the macrolide. The present of more conformation isomer and tautomer forms in solution led its ^{1}H-NMR spectrum become too complicated to be interpreted. To confirm the structure, the accurate mass measurements and elemental composition analysis of the diagnostic fragments (*m/z* 321, *m/z* 289, *m/z* 240, and *m/z* 196) were conducted (Table 4), which provided the support for this structure assignment.

M11 not only showed the same molecular ion and fragmentation ions as M10, but also displayed similar ion intensities as M10 in MS and MS/MS/CID spectra. The presence of the opened hemiketal ring ions (*m/z* 240 and *m/z* 196) suggested that M11 has

the same structure as M10, and was, most likely, an epimer of M10 with a different stereochemistry at C_{11} (Fig. 7).

Identification of M12. M12 was also an oxidative metabolite in the 'southern' region, as indicated by its molecular ion signal at *m/z* 1044 and the 'southern' fragment ions at *m/z* 606, *m/z* 588, *m/z* 562, *m/z* 544, *m/z* 530 and *m/z* 512 (Table 2 and Fig. 8a). The presence of the same group-2 ions (*m/z* 261, *m/z* 229, m/z 147, *m/z* 101, Table 2) as temsirolimus in the MS/MS spectra suggested that the right portion of the molecule from C_8 to C_1 and C_{36} to C_{32} was intact (Fig. 8a). Detection of the group-3 fragment ions at *m/z* 268 and *m/z* 250 in the MS/MS spectrum of M12 versus *m/z* 252 and *m/z* 234 for temsirolimus suggested that biotransformation had occurred in the left side of the 'southern' part, namely the C_9 to O_{24} region (Fig. 8a). Two unique ions at *m/z* 184 and *m/z* 144 with elemental compositions of $C_8H_{10}NO_4$ and $C_6H_{10}NO_3$ (based on accurate mass measurements), respectively, pointed to oxidation at the pipecolinyl ring (Fig. 8a). In the MS/MS/MS spectra, these two ions generated the fragment ions at *m/z* 168 and *m/z* 128, respectively, by eliminating oxygen, but not *m/z* 166 and *m/z* 126 from losing water, indicating that M12 was an N-oxide derivative of temsirolimus (Fig. 8a). This was supported by the observation of the downfiled shifts of H_{22} (δ 5.25 ppm) and H_{18} (δ 3.65 ppm) as compared with the parent compound (H_{22}: δ 5.12 ppm, overlapping with H_{25}) observed in the ^{1}H-NMR spectra (Figure 8b).

Identification of M13. In the negative ESI mass spectrum, M13 showed a molecular ion at *m/z* 1014 and fragmentation ions at *m/z* 437 and *m/z* 576, corresponding to a 'southern' desmethylation derivative of temsirolimus (Table 2). The MS/MS spectrum of the molecular ion gave the same group-3 ions, but different group-2 ions compared to

DMD Fast Forward. Published on May 31, 2007 as DOI: 10.1124/dmd.107.014746
This article has not been copyedited and formatted. The final version may differ from this version.

temsirolimus (Table 2), suggesting that the C_9-O_{24} region remained unchanged and biotransformation had occurred in the lower right region of the 'southern' part. The most likely desmethylation candidates were C_7 and C_{32} (Fig. 9a). The presence of the fragment ion at *m/z* 147, corresponding to the cleavage of C_8/C_9 and C_{35}/C_{36} in the 'southern' part, suggested that the C_7-O-methyl group was still intact and that C_{32}-O-desmethylation had occurred. This suggestion was supported by the disappearance of the fragment ion at *m/z* 101 and the appearance of the ion peak at *m/z* 87 from C_{34}/C_{35} cleavage of the 'southern' part. Therefore, the structure of M13 was proposed as C_{32}-O-desmethyl temsirolimus (Figure 9a). In the ^{1}H-NMR spectrum of M13, the disappearance of C_{32}-methoxyl proton signals at δ 3.24 and the downfield shifting of H_{31} as compared to temsirolimus further confirmed this assigned structure (Fig. 9b).

Biological Activity of the Major Metabolites. The biological activities of rapamycin and temsirolimus are dependent on the binding of the left-hand portion (C_8-C_{31}, the "binding domain") of the molecule to FKBP12 to form a complex, that in turn binds the mTOR protein through the remaining portion of the molecule (the "effector domain", Odagaki et al., 1997; Sedrani et al., 1999). The inhibtion of the mTOR pathway by FKBP12-rapamycin (or temsirolimus) blocks multiple downstream signals and leads to a general anti-proliferative effect. Therefore, any structural modification of the macrocyclic lactone ring (such as ring opening, hydroxylation of these two domains) could potentially affect the antineoplastic activities of the molecule. According to our proposed structures, the biotransformation locations of these metabolites were either in the "binding domain" (M10, M11, and M12), or in the "effector domain" (M8, M9, and M13), therefore, different antitumor activities from temsirolimus was expected. The

antitumor activity of the metabolites was evaluated in a cellular assay of LNCaP (a prostate carcinoma cell line) proliferation. Compared to temsirolimus, which showed an IC_{50} of 2 nM, these metabolites showed remarkably decreased activity (IC_{50} >100 nM) or absolutely no inhibitory activity (IC_{50} > 1000 nM), as seen in Table 5.

Discussion

Temsirolimus, an ester derivative of rapamycin, is a selective inhibitor of mTOR that showed clear clinical efficacy and excellent tolerability in the treatment of renal cancer patients. The i*n vitro* metabolism studies conducted with temsirolimus and human liver microsomes led to the formation of 15 metabolites as detected by LC-MS. Same as rapamycin, CYP3A4 was shown to be the major enzyme responsible for biotransformation through an inhibition study and by incubation with individual recombinant P450 enzymes. Such knowledge is of considerable clinical utility with regard to potential drug-drug interactions, as well as inter-individual differences in drug metabolizing capacities stemming from genetic polymorphisms, since CYP3A4 is involved in the biotransformation of around 60% of all the xenobiotics on the market today (Waxman et al., 1988; Guengerich, 1989; Thummel and Wilkinson, 1998), including cyclosporine, erythromycin, diazepam, nifedipine, estradiol, paclitaxel, and lovastatin. Co-administration of drugs that are substrates (such as erythromycin, clarithromycin, and lovastatin), inhibitors (such as troleanomycin and HIV-protease inhibitors), or induces (such as rifampin and carbamazepine) of CYP3A4 may affect the metabolic disposition of temsirolimus in humans. An earlier study on the effects of termsirolimus on patients with recurrent glioblastoma multiforme (Galanis et al., 2005), who were at the same time receiving P450-inducing anticonvulsants (EIACs, known to

increase CYP3A4), showed that the peak concentrations (Cmax) of temsirolimus and rapamycin decreased by approximately 73% and 47%, respectively, as compared to renal patients not receiving EIACs.

The 15 detectable metabolites were the monohydroxylation, demethylation, N-oxidation, and dihydoxylation / ring opening products of temsirolimus. Six major metabolites were identified to be 36-hydroxyl temsirolimus (M8), 35-hydroxyl temsirolimu (M9), 11-hydroxyl temsirolimus with an opened hemiketal ring (M10 and M11), N-oxide temsirolimus (M12) and 32-O-desmethyl temsirolimus (M13) by combined LC-MS, MS/MS, MS/MS/MS, and NMR spectroscopic methods. In humans, temsirolimus converts by hydrolysis to rapamycin, and both temsirolimus and rapamycin are subject to oxidative metabolism (Galanis et al., 2005). However, no rapamycin metabolites were observed in our study, most likely because the formation of rapamycin from temsirolimus in human liver microsomes was not extensive. Temsirolimus metabolites formed primarily via C-oxidation (aliphatic hydroxylation), O-demethylation, N-oxidation, and ring opening, which was similar to the metabolites found in pooled bile of rats after they were intravenously administered rapamycin (Wang el al., 1997). Besides seco-rapamycin, nine hydroxylated rapamycin and/or desmethylated rapamycin metabolites were detected in the same pooled rat bile. Although the structures of these metabolites were not identified, the hydroxylation and demethylation sites of three major biliary metabolites (m2, m10, and m13) were proposed at the regions of C_{32} to C_{36} and C_1 to C_{11} on the basis of LC-MS data, resembling to temsirolimus metabolites M8, M9, M10 and M11. Two ‘southern’ portion monohydroxylated rapamycin products were also found as the most abundant metabolites (~ 73.6% of total metabolites) from the blood of

kidney transplantation patients receiving rapamycin (Holt et al., 2003). Whether temsirolimus metabolites identified in our study share the same biotransformation locations with those *in vivo* rapamycin metabolites need to be further evaluated.

Although 41-O-desmethylation was the predominant metabolite of rapamycin in the incubation of rapamycin with human liver microsomes, this was not the case for temsirolimus. Such metabolic differences may be a consequence of C_{42}-O-esterification of temsirolimus. Introduction of the 2,2-bis- (hydroxymethyl)-propionate side chain at the C_{42} position resulted in significant steric hindrance, thus blocking CYP3A4 enzyme action on the 41-O-methyl group. It is worth to be mentioned that the major *in vitro* rapamycin metabolite, 41-O-desmethyl rapamycin, was not found in rat bile and kidney transplantation patients' blood at significant amounts according to Wang and Holt studies. This is probably due to that 41-O-desmethyl rapamycin underwent further oxidation and /or ring opening, and degraded to various products at very low amount. It is also possible that rapamycin (or temsirolimus) alters its structure conformation after binding to target proteins in *vivo*, which changes CYP3A4 action and results in a different biotransformation profile with that *in vitro*.

Incubation of temsirolimus with recombinant human CYP3A4 in the presence of a NADPH regenerating system reproduced almost all of the metabolites detected in human liver microsomes, so this technique was subsequently used to prepare the metabolites in a large-scale for isolation and analysis of the metabolites. Six major metabolites (M8 to M13) were isolated and purified, enabling unambiguous structural elucidation and bioactivity studies, and also providing useful reference standards for future *in vivo* metabolic studies.

As temsirolimus is a relatively complicated molecule, the structural elucidation of the metabolites was challenging. Combined LC-MS, MS/MS, MS/MS/MS and accurate mass measurements as well as NMR techniques provided powerful and reliable tools for metabolite structural elucidation. Temsirolimus usually is present in solution as two inter-changeable isomer forms, and the most proton signals overlapped in NMR spectrum. For metabolites, the hydroxylation and/or ring opening increases the complexity of proton NMR spectrum. The characteristic fragmentation pattern of temsirolimus in MS/MS and MS/MS/MS, and accurate mass measurements of the fragments can provide more structural information for those metabolites (such as M9, M10, and M11) with heavily overlapping and uninterpretable NMR data.

Acknowledgments. We are grateful to Dr. Melissa Lin and Yumin Gong for acquiring NMR data of temsirolimus metabolites.

References

Christians U, Sattler M, Schiebel HM, Kruse C, Radeke HH, Linck A, and Sewing K-FR (1992) Isolation of two immunosuppressive metabolites after in vitro metabolism of rapamycin. *Drug Metab. and Dispos.* **20:** 186-191.

Galanis E, Buckner JC, Maurer MJ, Kreisberg I, Ballman K, Boni J, Peralba JM, Jenkins RB, Dakhil SR, Morton RF, Jaeckle KA, Scheithauer BW, Dancey J, Hidalgo M, and Walsh DJ (2005) Phase II trial of temsirolimus (CCI-779) in recurrent glioblastoma multiforme: a north central cancer treatment group study. *J. Clin. Oncology* **23**: 5294-5304.

Guengerich FP (1989) Characterization of human microsomal cytochrome P450 enzymes. *Annu. Rev. Pharmacol. Toxicol*. **29:** 241-264.

Holt DW, Lee TD, Mckeown DA, Hicks D, Cai P, and Johnston A (2003) Relative proportions of sirolimus (rapamycin) metabolites in blood following kidney transplantation. *Presentation at 8th. International Congress of therapeutic drug monitoring & clinical toxicology* in Basel, Switzerland, Sept. 7.

Maurice M, Pichard L, Daujat M, Fabre I, Joyeux H, Domergue J, and Maurel P (1992) Effects of imidazole derivative on cytochromes P450 from human hepatocytes in primary culture. *FASEB J* **6:** 752-755.

Odagaki Y, and Clardy J (1997) Structural basis for peptidomimicry by the effector element of rapamycin. *J. Am. Chem. Soc.* **119:** 10253-10254.

Peralba JM, deGraffenried L, Friedrichs W, Fulcher L, Grunwald V, Weiss G, and Hidalgo M (2003) Pharmacodynamic evaluation of temsirolimus, an inhibitor of mTOR, in cancer patients. *Clin. Cancer Res.* **9:** 2887-2892.

Sattler M, Guengerich FP, Yun C, Christians U, and Sewing K-FR (1992) Cytochrome P450 and rat. *Drug Metab. and Dispos.* **20:** 753-761.

Sedrani R, Jones LH, Jutzi-Eme AM, Schuler W, and Cottens S (1999) Cleavage of the cyclohexyl-subunit of rapamycin results in loss of immunosuppressive activity. *Bioorg. Med. Chem. Let.* **9:** 459-462.

Sehgal SN (1995) Rapamune (sirolimus, rapamycin): an overview and mechanism of action. *Ther. Drug Monit.* **17:** 660-665.

Sehgal SN, Molnar-Kimber K, Ocain TD, and Weichman BM (1994) Rapamycin: a novel immunosuppressive macrolide. *Med. Res. Rev.* **14:**1-22.

Thummel KE and Wilkinson GR (1998) In vitro and in vivo drug interactions involving human CYP3A. *Annu. Rev. Pharmacol. Toxicol*. **38:** 389-430.

Wang CP, Chan KW, Schiksnis RA, Scatina JA, and Sisenwine SF (1994) High performance liquid chromatographic isolation and spectroscopic characterization and immunosuppressive activities of two rapamycin degradation products. *J. Liq. Chrom.* **17:** 3383-3392.

Waxman DJ, Attisano C, Guengerich FP and Lapenson DP (1988) Human Liver microsomal steroid hormone 6b-hydroxylase cytochrome P450 enzyme. *Arch. Biochem. Biophys.* **263:** 424-436.

Footnotes

Person to receive reprint requests: Ping Cai, Wyeth Research, Chemical and Pharmaceutical Development, Building 250/229, 401 N. Middletown Road, Pearl River, NY 10965.

Legends for figures

Fig. 1. Representative HPLC chromatograms of temsirolimus incubation products in (1a) HLM control; (1b) HLM / NADPH regenerating system; (1c) recombinant 3A4 / NADPH regenerating system; (1d) recombinant 3A4 control.

Fig. 2. Expanded semi-preparative HPLC chromatograms of temsirolimus incubation products in HLM/NADPH (top) and in recombinant CYP3A4/NADPH (bottom).

Fig. 3. Effect of ketoconazole on the formation of temsirolimus metabolites. The data shown are the average of duplicates.

Fig. 4. MS/MS spectrum of temsirolimus and the fragmentation assignments.

Fig. 5a. Proposed structure of M8 and the fragmentation assignments (observed fragment ions are listed in Table 2).

Fig. 5b. An expanded ^{1}H-NMR spectrum of M8 compared with that of temsirolimus.

Fig. 6. Proposed structure of M9 and the fragmentation assignments (observed fragment ions are listed in Table 2).

Fig. 7. Proposed structure of M10 and M11, and the fragmentation assignments (observed fragment ions are listed in Table 2).

Fig. 8a. Proposed structure of M12 and the fragmentation assignments (observed fragment ions are listed in Table 2).

Fig. 8b. An expanded ^{1}H-NMR spectrum of M12 compared with that of temsirolimus.

Fig. 9a. Proposed structure of M13 and the fragmentation assignments (observed fragment ions are listed in Table 2).

Fig. 9b. An expanded ^{1}H-NMR spectrum of M12 compared with that of temsirolimus.

DMD Fast Forward. Published on May 31, 2007 as DOI: 10.1124/dmd.107.014746
This article has not been copyedited and formatted. The final version may differ from this version.

Table 1. LC-MS comparison of temsirolimus metabolic products from human liver microsomes and from recombinant CYP3A4

Products from HLM (Retention Time)[a]	$[M-H]^-$ m/z[b]	Products from CYP3A4 (Retention Time)[a]	$[M-H]^-$ m/z[b]
Peak 1-2 (29.8-31.2 min)	1060, 1058	Peak 1-2 (31.0-31.9 min)	1060, 1046
Peak 3-4 (35.7-36.2 min)	1060, 1046, 1014	Peak 3 (32.4 min)	1030
Peak 5 (3638.2 min)	1030	Peak 4 (35.7 min)	1014
Peak 6 (40.1 min)	1026	Peak 5-6 (38.3-39.8 min)	1026, 1028
Seco-temsirolimus (43.9 min)	1028	Seco-temsirolimus (44.1 min)	1028
Peak 7 (47.0 min)	1030	Peak 7 (47.6 min)	1030
M8 (54.5 min)	1044	M8 (54.6 min)	1044
M9 (58.0 min)	1044	M9 (58.3 min)	1044
M10 (61.2 min)	1044	M10 (61.8 min)	1044
M11 (64.4 min)	1044	M11 (64.9 min)	1044
Peak 11' (66.2 min)	1030	-----	
M12 (69.8 min)	1044	M12 (69.8 min)	1044
M13 (83.3 min)	1014	M13 (83.1 min)	1014
M14 (87.4min)	1028	-----	
Temsirolimus[c] (87.9-90 min)	1028	Temsirolimus (88.2-90 min)	1028

[a] retention time in semi-preparative HPLC
[b] all in negative ESI-MS
c like rapamycin, temsirolimus exists in two isomer forms in solution.

DMD Fast Forward. Published on May 31, 2007 as DOI: 10.1124/dmd.107.014746
This article has not been copyedited and formatted. The final version may differ from this version.

Table 2. MS/MS fragmentation data of temsirolimus and its major metabolites

Metabolite	$[M-H]^-$	Fragment Ions, *m/z*		
	m/z	'northern' ions	'southern' ions[a]	
temsirolimus	1028.7	437, 407, 389, 371	590, 546, 528, 514, 496	(group-1)
			261, 229, 147, 101	(group-2)
			252, 234, 168, 128	(group-3)
M8	1044.6	437, 407, 389, 371	606, 562, 544, 530, 512	(group-1)
			277, 259, 245, 227, 163, 101	(group-2)
			252, 234, 168, 128	(group-3)
M9	1044.6	437, 407, 389, 371	606, 562, 544, 530, 512	(group-1)
			277, 259, 245, 227, 147, 101	(group-2)
			252, 234, 168, 128	(group-3)
			504, 472, 175	(unique group)
M10	1044.6	437, 407, 389, 371	606, 562, 544, 530	(group-1)
			261, 229, 147, 101	(group-2)
			168, 128	(group-3)
			321, 289, 240, 196	(unique group)
M11	1044.6	437, 407, 389, 371	606, 562, 544, 530	(group-1)
			261, 229, 147, 101	(group-2)
			168, 128	(group-3)
			321, 289, 240, 196	(unique group)
M12	1044.6	437, 407, 389, 371	606, 562, 544, 530, 512	(group-1)
			261, 229, 147, 101	(group-2)
			268, 250, 184, 168, **144**, 128	(group-3)
M13	1014.6	437, 407, 389, 371	576, 532, 514, 500, 482	(group-1)
			247, 229, 147, **87**	(group-2)
			252, 234, 168, 128	(group-3)

[a] the numbers in bold are the *m/z* of key fragment ions used in structural elucidation.

DMD Fast Forward. Published on May 31, 2007 as DOI: 10.1124/dmd.107.014746
This article has not been copyedited and formatted. The final version may differ from this version.

Table 3. Observed and calculated *m/z* values of the unique ions in the MS/MS spectrum of M9

Measured [a] *m/z*	Calculated *m/z*	Elemental composition	Error (mDa)
504.2618	504.2603	$C_{27}H_{38}NO_8$	+1.5
472.2351	472.2341	$C_{26}H_{34}NO_7$	+1.0
175.1112	175.1128	$C_{12}H_{15}O$	-1.6

[a] accurate mass measurements were made using the molecular ion of *m/z* 1044.5897 and the known fragment ion of *m/z* 168.0661 as references.

DMD Fast Forward. Published on May 31, 2007 as DOI: 10.1124/dmd.107.014746
This article has not been copyedited and formatted. The final version may differ from this version.

Table 4. Observed and calculated *m/z* values of the unique ions in the MS/MS spectrum of M10

Measured [a] *m/z*	Calculated *m/z*	Elemental composition	Error (mDa)
321.2065	321.2060	$C_{19}H_{29}O_4$	+0.5
289.1825	289.1800	$C_{18}H_{25}O_3$	+2.5
240.0851	241.0872	$C_{11}H_{14}NO_5$	-2.1
196.0987	196.0974	$C_{10}H_{14}NO_3$	+1.3

[a] accurate mass measurements were made using the molecular ion of *m/z* 1044.5897 and the known fragment ion of *m/z* 168.0661 as references.

DMD Fast Forward. Published on May 31, 2007 as DOI: 10.1124/dmd.107.014746
This article has not been copyedited and formatted. The final version may differ from this version.

Table 5. Inhibitory activity of temsirolimus metabolites against LNCaP cell proliferation

Sample	IC_{50} (nM)
temsirolimus	2
seco-temsirolimus	~5000
M8	~1000
M9	~100
M10	~200
M11	~200
M12	~1000
M13	~1000

DMD Fast Forward. Published on May 31, 2007 as DOI: 10.1124/dmd.107.014746
This article has not been copyedited and formatted. The final version may differ from this version.

Figure 1.

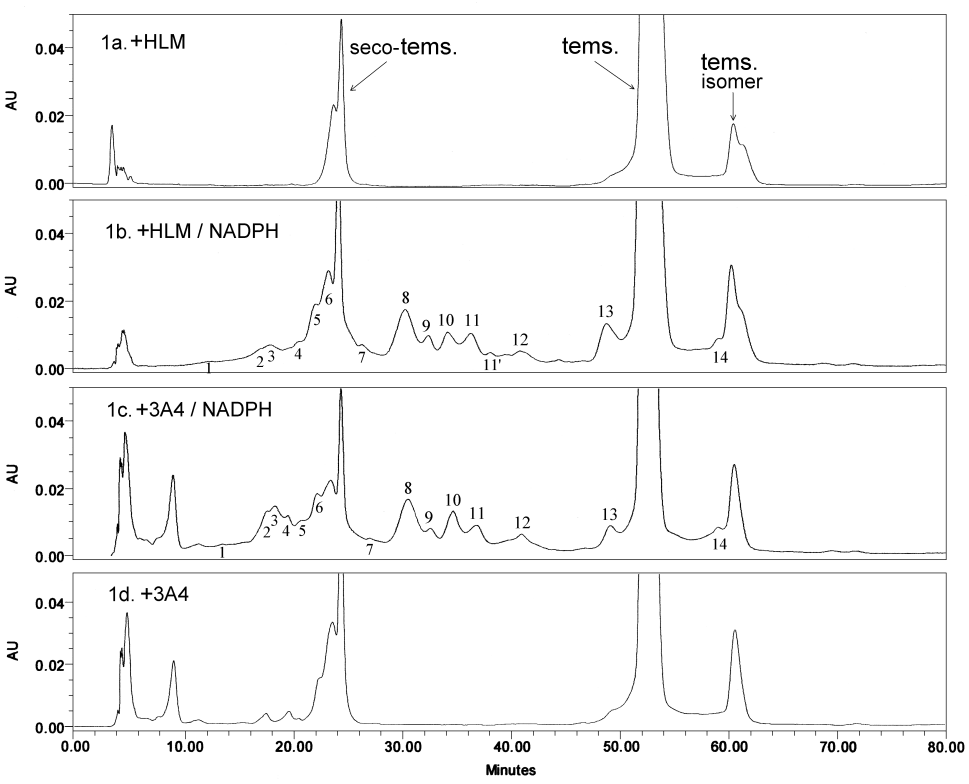

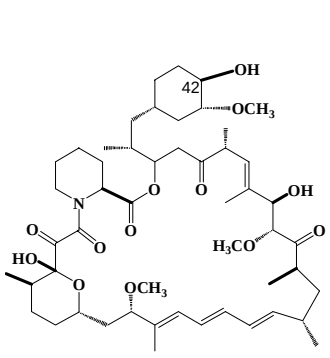

Rapamycin

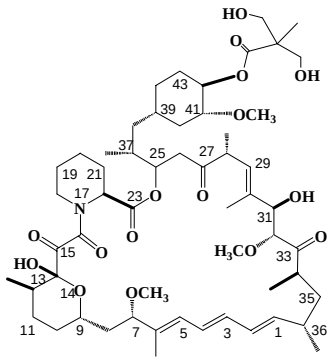

Temsirolimus

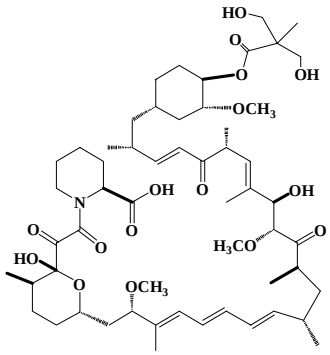

Seco-temsirolimus

DMD Fast Forward. Published on May 31, 2007 as DOI: 10.1124/dmd.107.014746
This article has not been copyedited and formatted. The final version may differ from this version.

Figure 2.

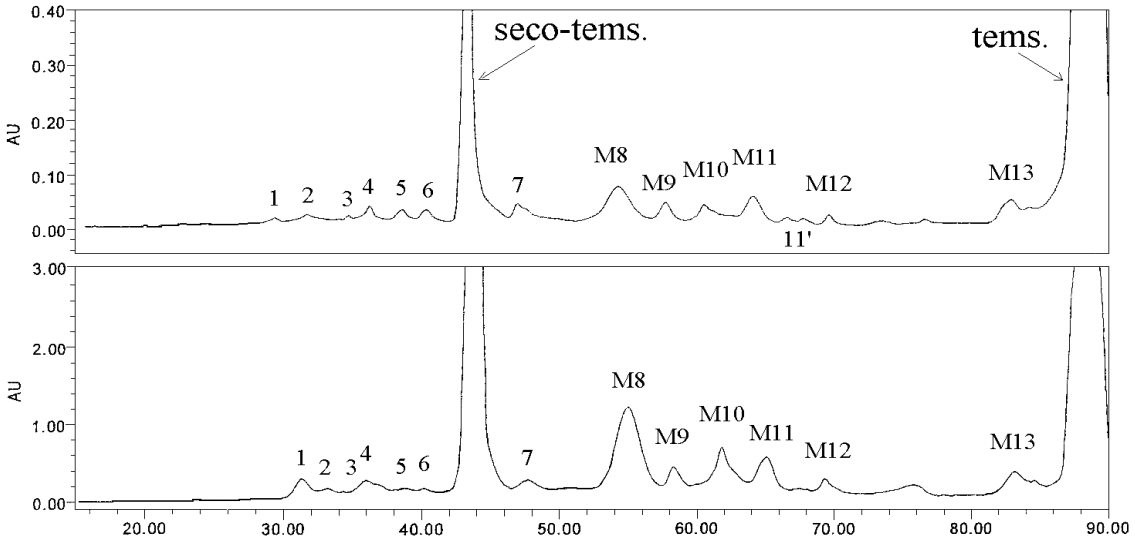

DMD Fast Forward. Published on May 31, 2007 as DOI: 10.1124/dmd.107.014746
This article has not been copyedited and formatted. The final version may differ from this version.

Figure 3.

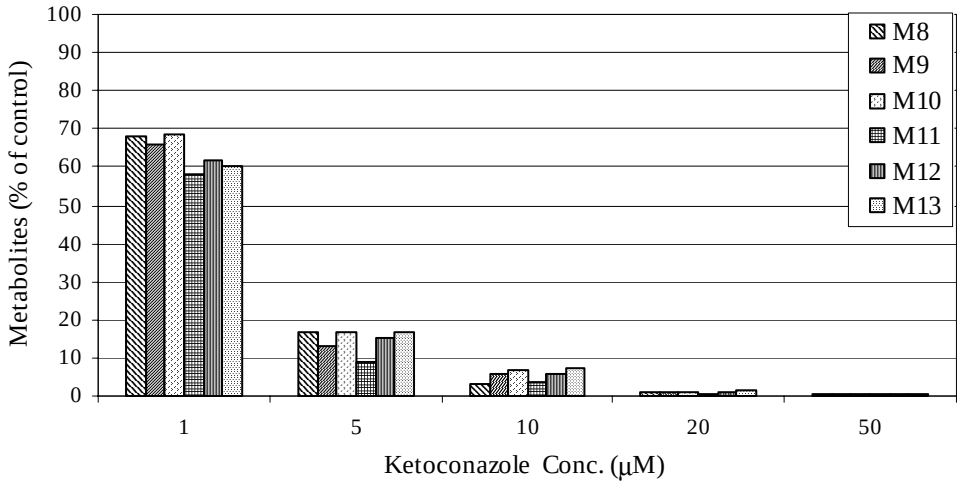

DMD Fast Forward. Published on May 31, 2007 as DOI: 10.1124/dmd.107.014746
This article has not been copyedited and formatted. The final version may differ from this version.

Figure 4.

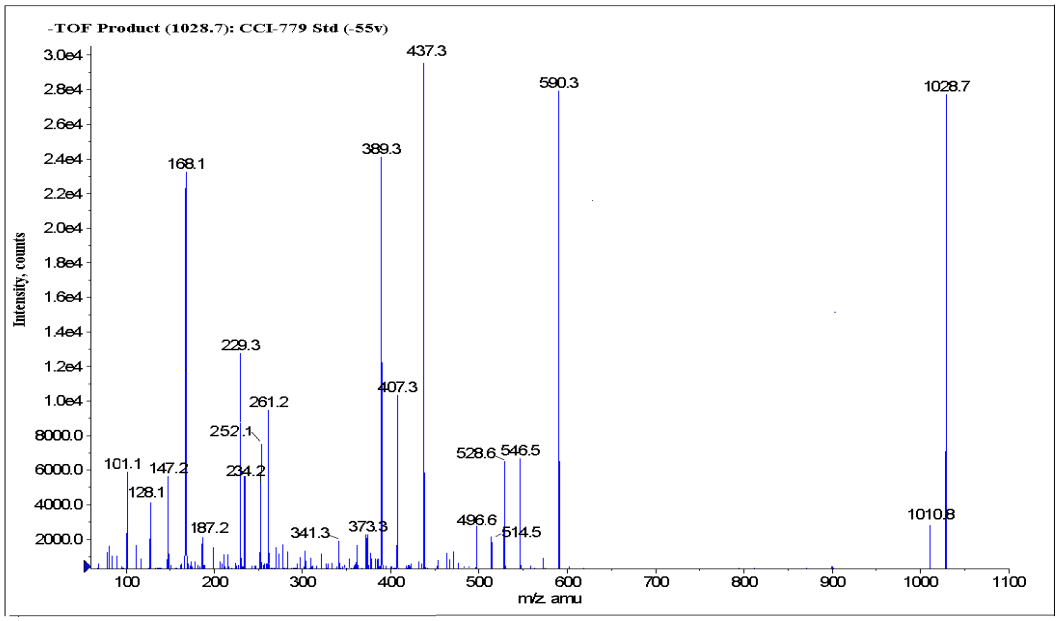

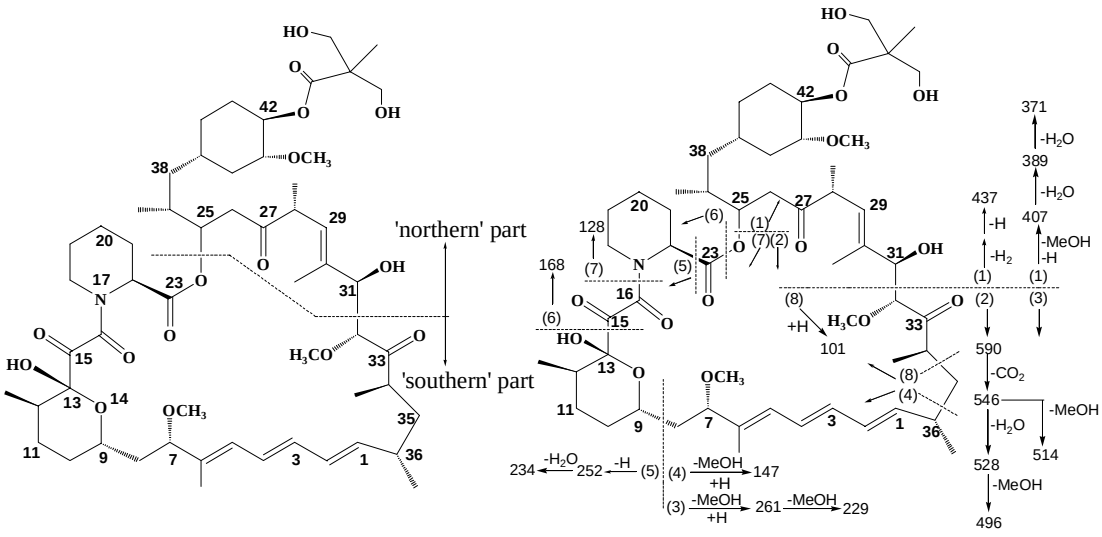

DMD Fast Forward. Published on May 31, 2007 as DOI: 10.1124/dmd.107.014746
This article has not been copyedited and formatted. The final version may differ from this version.

Figure 5a.

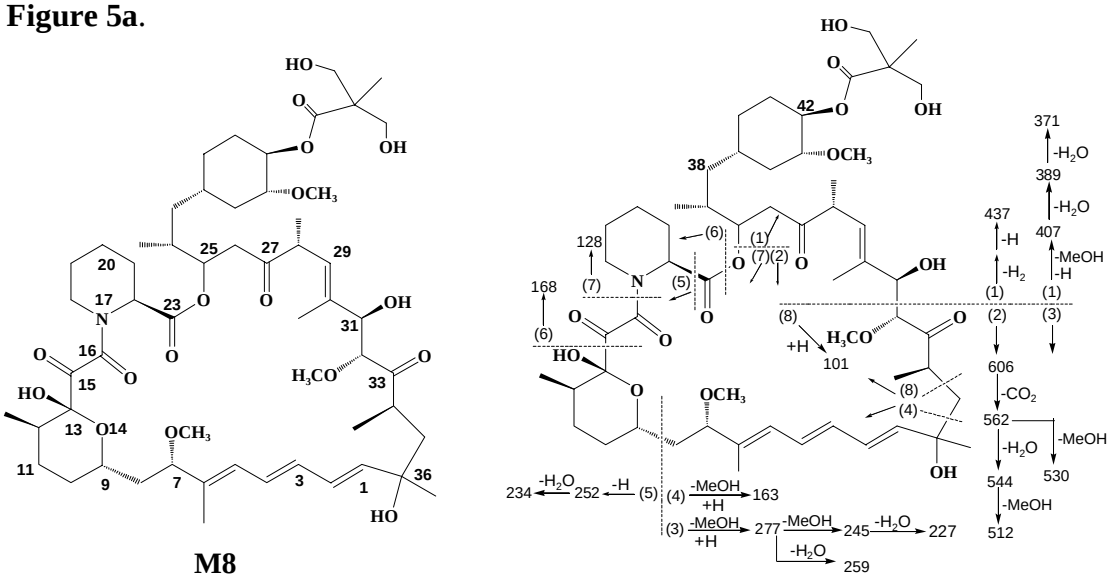

M8

DMD Fast Forward. Published on May 31, 2007 as DOI: 10.1124/dmd.107.014746
This article has not been copyedited and formatted. The final version may differ from this version.

Figure 5b

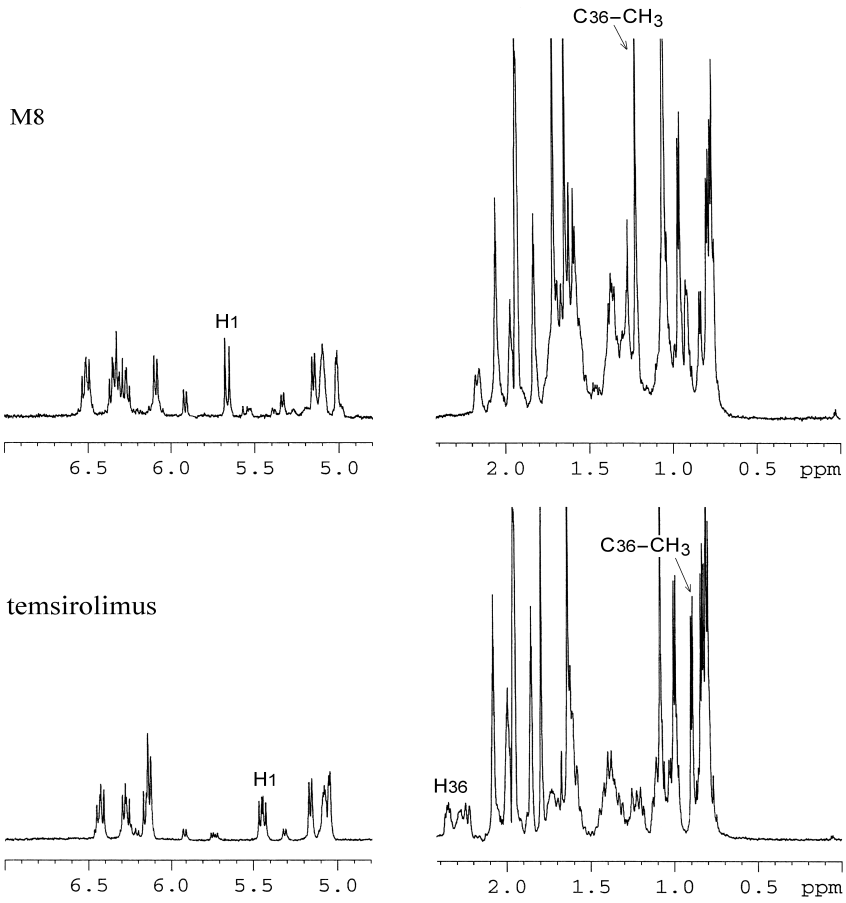

DMD Fast Forward. Published on May 31, 2007 as DOI: 10.1124/dmd.107.014746
This article has not been copyedited and formatted. The final version may differ from this version.

Figure 6.

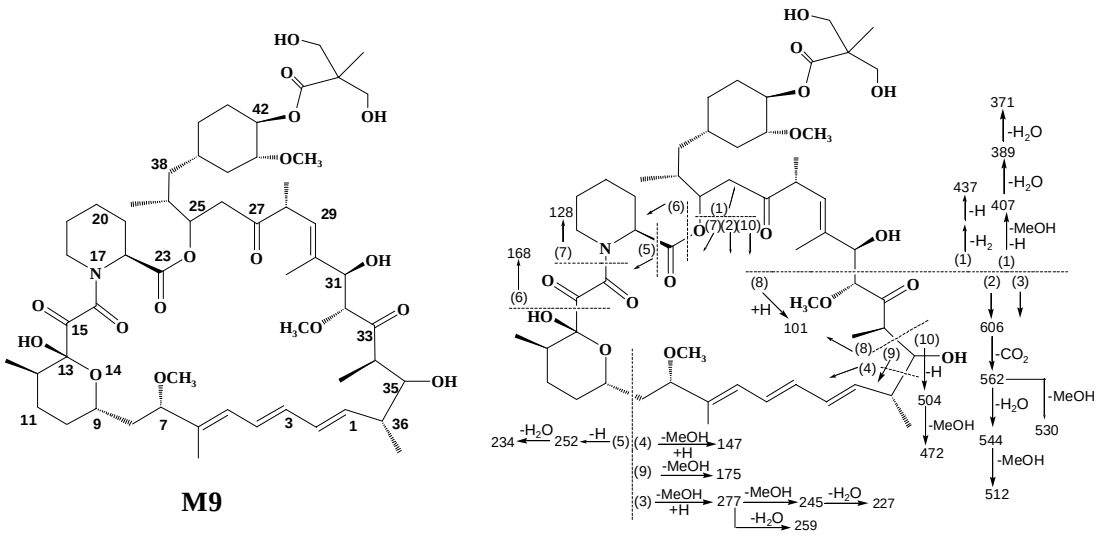

DMD Fast Forward. Published on May 31, 2007 as DOI: 10.1124/dmd.107.014746
This article has not been copyedited and formatted. The final version may differ from this version.

Figure 7.

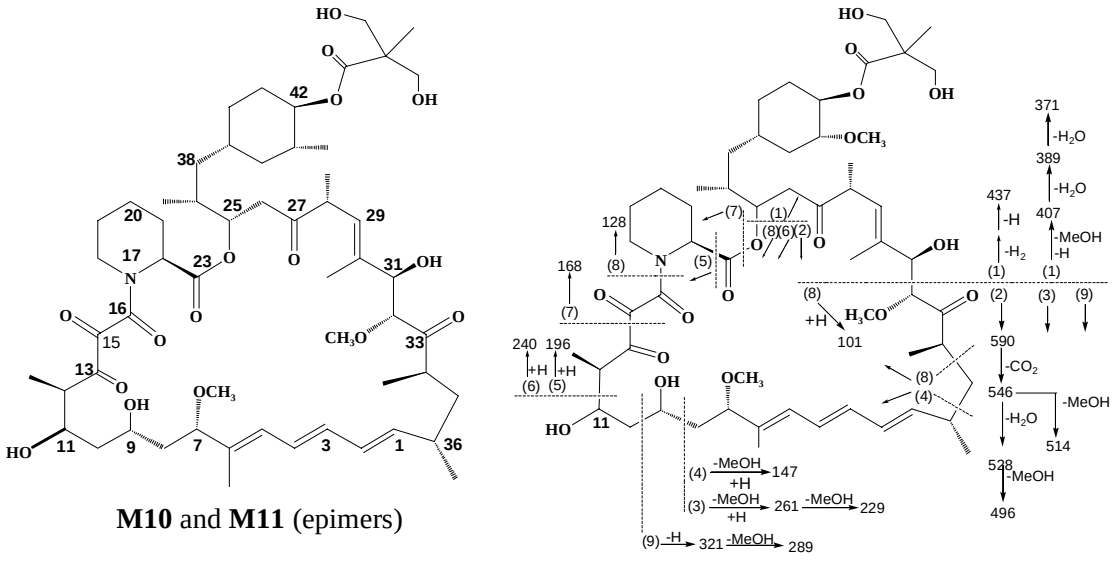

M10 and **M11** (epimers)

DMD Fast Forward. Published on May 31, 2007 as DOI: 10.1124/dmd.107.014746
This article has not been copyedited and formatted. The final version may differ from this version.

Figure 8a.

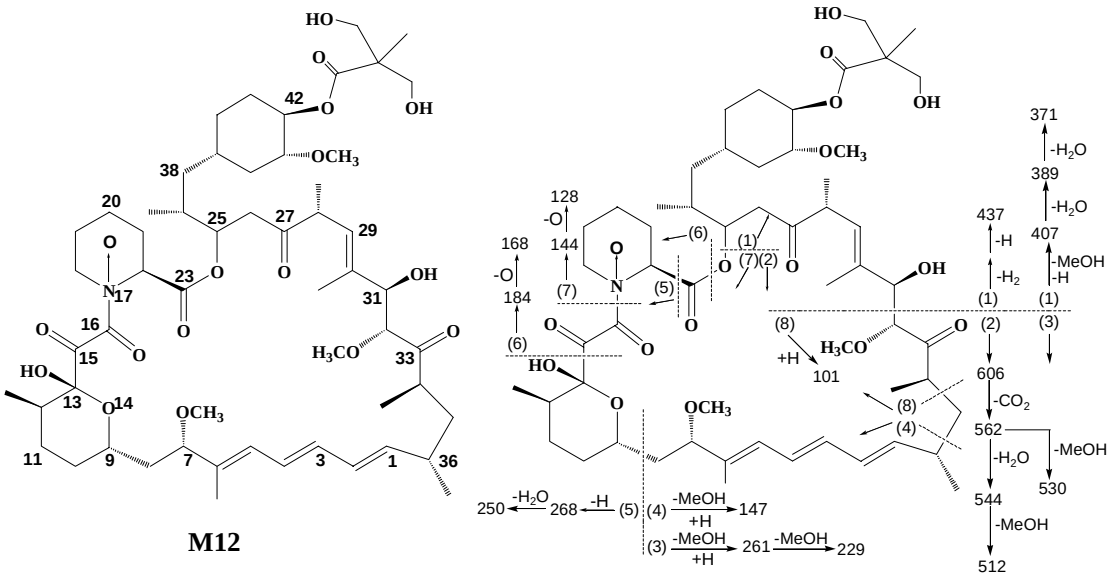

DMD Fast Forward. Published on May 31, 2007 as DOI: 10.1124/dmd.107.014746
This article has not been copyedited and formatted. The final version may differ from this version.

Figure 8b

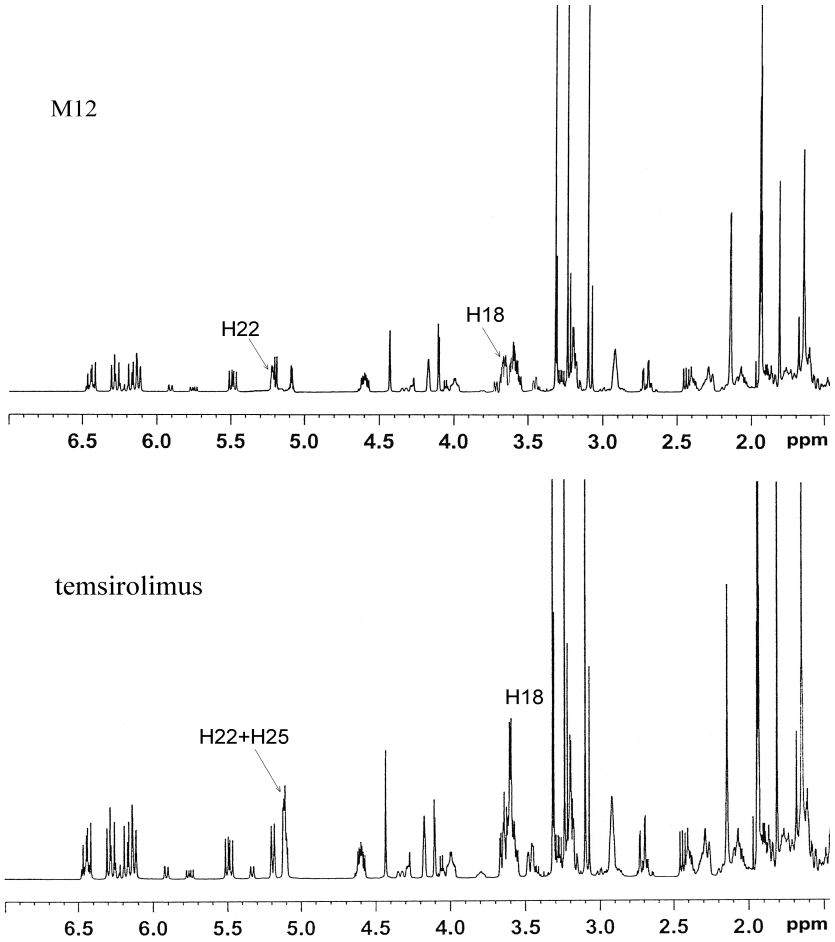

DMD Fast Forward. Published on May 31, 2007 as DOI: 10.1124/dmd.107.014746
This article has not been copyedited and formatted. The final version may differ from this version.

Figure 9a.

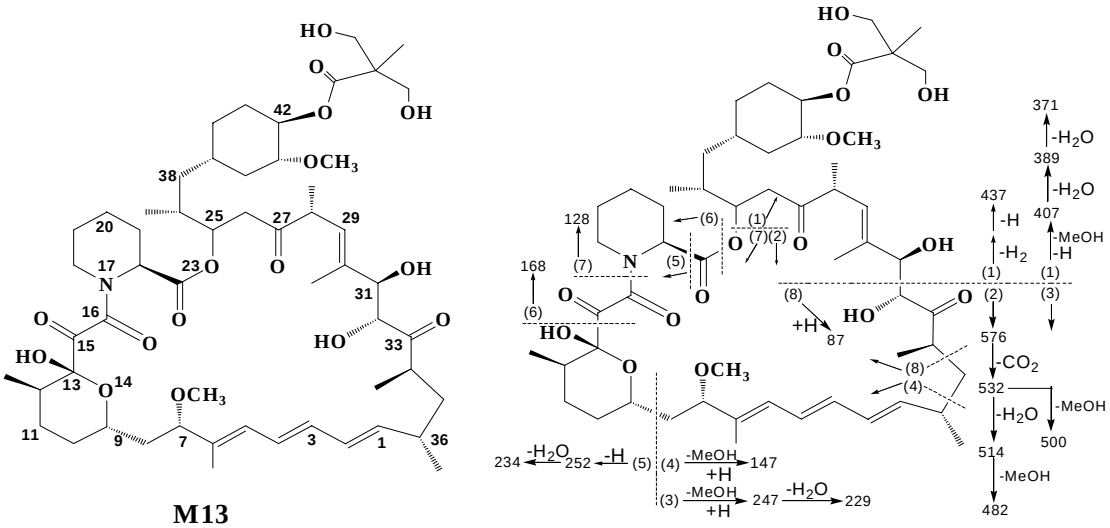

DMD Fast Forward. Published on May 31, 2007 as DOI: 10.1124/dmd.107.014746
This article has not been copyedited and formatted. The final version may differ from this version.

Figure 9b